JME

Journal of Mining & Environment,
Vol. 9, No. 4, 2018, 1049-1064.
DOI: 10.22044/jme.2018.7201.1572

Evaluating performance of natural sepiolite and zeolite nanoparticles for nickel, antimony, and arsenic removal from synthetic wastewater

R. Dabiri* and E. Amiri Shiraz

Department of Geology, Mashhad Branch, Islamic Azad University, Mashhad, Iran

Received 24 June 2018; received in revised form 21 August 2018; accepted 25 August 2018
Corresponding author: r.dabiri@mshdiau.ac.ir (R. Dabiri).

Abstract
This paper describes a preliminary study of the adsorption of toxic elements from synthetic wastewater in a batch mode. Clay minerals have been highly considered as inexpensive available adsorbents that adapt with the environment due to a special level and a high potential of adsorption. In the present research work, low-cost natural minerals of speiolite from the Iliato mine (located in NE Iran) and zeolite from the Aftar mine (located in north of Iran) are used to remove nickel(II), antimony(III), and arsenic(V) from synthetic wastewater. The adsorption experiments are conducted by varying the initial concentrations of the elements, pH values, adsorption times, and adsorbent dosage. The experimental isotherm data is analyzed using the Langmuir and Freundlich equations. Concerning a higher Langmuir coefficient R^2 in nickel and antimony, the mechanism of adsorption of these elements is mono-layer and homogenous. Based on the Freundlich model, adsorption of arsenic is multi-layer and heterogeneous. The kinetic studies show that the Ni, Sb, and As adsorption mechanism is well-described by a pseudo-second-order kinetic model. The thermodynamic parameters indicate that the adsorption process has an exothermic character and is more feasible with decreasing temperature. Based on the experimental results, it can be concluded that natural sepiolite and zeolite has the potential of application as an efficient adsorbent for the removal of toxic elements from synthetic wastewater.

Keywords: *Adsorption, Sepiolite and Zeolite Nanoparticles, Toxic Elements, Isotherm, Kinetic.*

1. Introduction

Water pollution is a global challenge that has increased in both the developed and developing countries, undermining the economic growth as well as the physical and environmental health of billions of people [1]. Contaminative causes are various, and the most important contaminants are toxic elements such as nickel, antimony, and arsenic. Such elements enter water due to natural factors (lithogenic) such as solution of sediments or anthropogenic factors such as development of industries, population growth, and production of industrial, urban, household, and agricultural wastewater [2-4]. Toxic elements accumulate in the environment due to their stability, and contaminate water and soil. These elements can lower the energy levels and damage the functioning of the brain, lungs, kidneys, liver, blood composition, and other important organs [5]. Therefore, it is vital to remove such contaminative metals from water and soil. Several processing techniques including the membrane processing, ion exchange, solvent extraction, reverse osmosis, phytoremediation, and electrolytic methods are available to reduce the concentration of toxic elements in wastewater [6-10]. Adsorption is a very effective separation technique in terms of the initial cost, simplicity of design, ease of operation, and insensitivity to toxic substances [11, 12]. Due to the economic considerations, natural minerals are promising alternatives as adsorbents for wastewater treatment [13]. Sepiolite and zeolite are the most promising adsorbents among the minerals with different adsorption properties [14]. Substitution

of silicium cations (Si^{+4}) in the tetrahedral layers of sepiolite via aluminum ions (Al^{+3}) and creation of negative charge is a proper place for adsorption of cations. Also a considerable number of silanol (Si-OH) is seen in this mineral due to discontinuity of the external silicate planes [15, 16]. Zeolites are aqueous aluminosilicates, and their tectosilicate structure is tetrahedral; their center is mostly occupied by silicium or aluminum, and oxygen atoms are at the four corners. The channels and holes are formed by connection of these tetrahedrons, and they are proper places for water, liquids, gases, and molecules [17, 18]. Zeolites have a special crystalline structure, and, particularly, they are able to substitute Si^{+4} via Al^{3+}, which causes a negative charge. The alkaline and alkaline-earth ions such as K^+, Na^+, Ca^{2+}, and Mg^{2+} enter the zeolite network and increase ion exchange [19, 20]. The use of nanoparticles for removal of environmental contaminants has been considered as one of the newest methods for the removal of toxic elements throughout the world [21, 22]. The objective of this work was to study the ability of natural sepiolite and zeolite to adsorb nickel, antimony, and arsenic. The adsorption of nickel, antimony, and arsenic on natural minerals was studied on the basis of batch experiments. The influence of the parameters mass of adsorbent, contact time, sorbate concentration, pH, and presence of competing ions and temperature was examined. The empirical models Freundlich and Langmuir were used to fit the adsorption isotherms.

2. Materials and methods

2.1. Chemicals and preparation of adsorbents

A combination of sepiolite and zeolite was used as the adsorbent in the present work. The zeolite sample was prepared from the Aftar mine located in Semnan (north of Iran) and the sepiolite sample was prepared from the Iliato mine located in Fariman (NE Iran). At first, the speiolite and zeolite samples (50%) were grinded for 10 min using a grinding machine and a planetary mill (speed, 2800 rpm); the planes were made of carbide tungsten. Then in order to prepare the nanoparticles, they were placed in a ball mill, model M-200 (ball weight, 6.293 g; ratio of 1:20; number of revolutions, 260 rpm; the balls were made of stainless steel) in the central laboratory of the Ferdowsi University in Mashhad [23]. In order to determine and analyze the size of particles, the VASCO particle size analyzer of the Ferdousi University was used. An ultrasonic machine, model Parsonic 2600, was used to prevent the agglomeration of particles. In order to determine the type of minerals, crystalline phase, chemical compound, and crystallinity degree, the powdered samples were XRD-analyzed in the Zarazma laboratory using a Philips analyzer, model PW 1800, with a voltage of 40 KV, a current of 30 mA, and a copper tube. Moreover, the Brunauer-Emmett-Teller (BET) analysis was used to study the specific surface area and pore size distribution. In order to study the structure of particles, SEM analysis was used. In this direction, the images were prepared by an electronic microscope with a magnification of up to 100000 times. The machine used here was VEGA//TESCAN-XMU with 150 KW voltages. The analysis was done in the Research Center of Mashhad. The FT-IR spectra were obtained in the 4000-400 cm^{-1} region using the KBr pellet technique (1% KBr sample). The pH_{PZC} (point of zero charge) at which the adsorbent was neutral in the aqueous suspension was determined following the Lopez-Ramon procedure [24]. In this method, 50 mL of 0.01 M NaCl solutions were filled in closed Erlenmeyer flasks under agitation at room temperature (about 25 °C). The pH of each solution was initially fixed at a value lying from 2 to 12 by adding 0.1 M HCl or 0.1 M NaOH solution. Then 0.1 g of the solid adsorbent was added to each flask and the final pH value was measured after 48 h. pH_{PZC} was localized at the point where the curve pH_{final} versus $pH_{initial}$ intersected the first bisector.

2.2. Preparation of solutions

Combinations of nickel(II) nitrate ($Ni(NO_3)_2.6H_2O$) with a molar mass of 260.81 g/mol, antimony trichloride ($Sb(Cl)_3$) with a molar mass of 228.11 g/mol, and arsenate hydrogen sodium ($Na_2HAsO_4.7H_2O$) with a molar mass of 312.01 g/mol (produced by Titrachem Co.) were used to prepare the synthetic wastewater. In order to prepare the solutions with different concentrations, 1.2385 g of nickel(II) nitrate and 1.041 g of arsenate hydrogen sodium were disolved in a volumetric flask containing 500 mL distilled water, and a 500 mg/L solution was made. In order to prepare the antimony solution, 0.1835 g of antimony trichloride was disolved in 5 M chloridrice acid in a 100 mL flask. Then the solutions with the different concentrations of 1, 5, 10, and 5000 mg/L were prepared from the main solution for the adsorption tests. The solutions of nitric acid and soda (1 and 0.1 normal) were prepared for pH adjustment.

2.3. Batch experiments

The adsorption experiments were conducted by a batch mode. In order to test each parameter, 100 mL of the solutions with different concentrations (50 mL for the adsorption experiment and 50 mL for the control solution) were prepared. After adjustment of pH with different adsorbent doses in different times (based on Table 1), the solution was placed on a stirrer (with a magnetic stirrer) with 110 rpm at 16.5-19 ^{o}C, and a 0.22-micron syringe filter was used to separate the adsorbent. The concentration amount adsorbed by the elements was measured by the ICP-OES method. All experiments were done by a step technique to determine the favorable conditions; in each stage, one parameter was variable and the others were constant. Concerning the highest percent of removal of the variable parameters, a favorable amount was determined for each parameter.

In all experiments, the adsorption capacity and intensity graphs were plotted using Excel in order to study the parameters. The effects of the parameters involved were compared. In addition, the following formulas were used to plot the graphs of percent removal of elements and their adsorption capacity. In these formulas, C_0 is the primary concentration, Ce is the final concentration of the elements in the solution, q_e is the adsorption capacity of the elements, V is the solution volume in L, and m is the amount of adsorbent in g/L [25].

$$R(\%) = \frac{C_0 - C_e}{C_0} \times 100 \quad (1)$$

$$q_e = \frac{(C_0 - C_e) \times V}{m} \quad (2)$$

The adsorption mechanism in clay minerals is based upon the adsorption and ion exchange [26]. In the present work, in order to study the cations exchanged in the adsorption experiments, a number of cations effective on the exchange of the toxic elements nickel, antimony, and arsenic were determined concerning the structural formulas of sepiolite and zeolite. Their concentrations were measured in the solution in favorable conditions before and after adsorption using the ICP-OES method, and the graphs were plotted.

Table 1. Variable parameters involved in adsorption experiment.

Parameter	Amounts of variable parameters			
pH	2	4	6	6
Time (min)	5	15	30	30
Concentration (mg/L)	1	5	10	10
Adsorbent dose (g/L)	1	2	3	3

2.4. Adsorption isotherms

The Langmuir and Freundlich models are commonly used to describe the adsorption equilibrium data. They were applied to the experimental results. Therefore, a correlation graph was plotted using Excel at 23 °C and concentrations of 1, 5, 10, 50, and 100. Adsorption isotherms are the mathematic models that describe the distribution of adsorbate between the liquid and gas phases based on the hypotheses attributed to the homogeny and heterogeneity of the solid surface, type of envelope, and competition of adsorbates [27]. The Langmuir sorption isotherm was applied to the equilibrium sorption assuming a mono-layer sorption onto a surface with a finite number of identical sites [12]. Even double layer adsorption could be obtained by the optimized equations [28]. The Langmuir linear equations were used in this research work as follow:

$$\frac{C_e}{q_e} = \frac{1}{bq_m} + \frac{1}{q_m} C_e \quad (3)$$

$$\frac{1}{q_e} = \frac{1}{q_m b} \times \frac{1}{C_e} + \frac{1}{q_m} \quad (4)$$

In Equations 3 and 4, C_e represents the equilibrium concentration of solution in mg/L, qe is the amount of solute adsorbed (mg/g) at equilibrium, q_m (in mg/g) and b (in L/mg) are the adsorption capacity and adsorption energy, respectively, Q_m is the inverse of y-intercept, and b is the width to slope ratio. One non-dimensional coefficient known as separation factor (R_L) is used in the Langmuir model to express the main feature of the isotherm; it is also used to evaluate the adsorbent in adsorption, and shows the adsorption condition. For this purpose, the separation factor is defined as follows:

$$R_1 = \frac{1}{(1 + bC_0)} \quad (5)$$

where C_0 is the initial concentration in mg/L and b is a constant. Based on the separation factor R_L, the isotherm status is interpretable. If $0 < R_L < 1$, the adsorption process will be favorable and if $R_L = 1$, it will be linear; if $R_L = 0$, it will be

irreversible, and in the case of $R_L > 1$, it is not favorable [29]. Also in order to study the Freundlich adsorption isotherm that is based upon a multi-layer adsorption on heterogeneous surfaces with unequal energy [30], the adsorption was studied according to Equation 6.

$$\log q_e = \log K_F + \frac{1}{n}\log C_e \quad (6)$$

where Ce is the concentration of elements at equilibrium, K_f is the adsorption capacity, and n is the adsorption power of the Freundlich constants. 1/n shows a favorable adsorption and the heterogeneity of the surface. If $1/n < 1$, the surface will show the highest heterogeneity, if $1/n = 1$, it will be linear, and in the case of $1 < n < 10$, the adsorption will be favorable. The values for K_f and n can be determined as y-intercept and linear slope in Log q_e graph against Log C_e graph, respectively. If the graph obtained from the plotted point is linear, it will be fitted with the Freundlich isotherm model [31].

3. Results and discussion

3.1. XRD analysis results

In order to determine the type of particles, XRD analysis was done on the powdered samples. Then two graphs were obtained (Figure 1). As shown in the XRD results, the main phase of combination is zeolite clinopetilolite with the chemical formula of ($KNa_2Ca_2(Si_{29}Al_7)O_{72}.24H_2O$) with quartz ($SiO_2$) consisting of the minor phase (Figure 1-a). In the graph shown in Figure 1-b, the main phase is sepiolite with the chemical formula of ($Mg_4Si_6O_{15}(OH)_2.6H2O$), and the minor phase is a little amount of quartz, dolomite, $CaMg(CO_3)_2$, montmorillonit.xH2O, and $CaO.2(Al,Mg)_2Si_4O_{10}(OH)_2$. As it can be seen in the figure, zeolite clinopetillolite is rich in sodium, calcium, and potassium; and sepiolite is rich in magnesium. The sharp points and clear peaks in the above-mentioned graphs are due to the crystallinity of the samples and low width of the peaks (Figure 1).

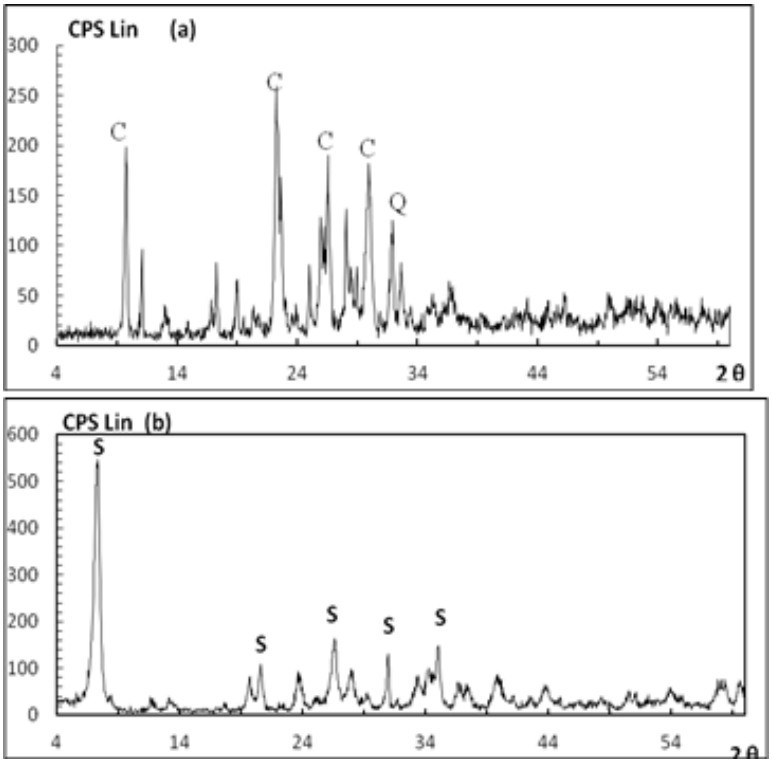

Figure 1. Patterns in XRD spectra of the powdered samples: (a) zeolite and (b) sepiolite (C: Clinoptilolite, Q: quartz, S: sepiolite).

3.2. Particle size statistics

As it can be seen in Figure 2, the skewed curve is negative and deviation towards the particles is less than 100 nm. More than 90% of the particles are less than 100 nm. The mean size of the particles is 72.05 nm. The specific surface area, total pore volume, and mean pore diameter of sepiolite (S.04) and zeolite (Z.01) were measured using the BET technique. Table 2 shows the results of the BET method.

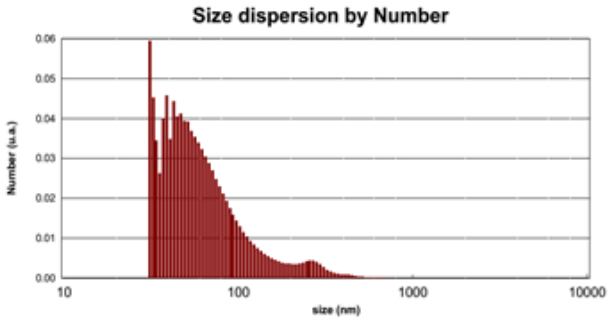

Figure 2. A view of graphs of analysis and distribution of nanoparticles of sepiolite and zeolite (DLS). Graph of particle size distribution in terms of particle numbers.

Table 2. Results of BET analysis.

Sample	Specific surface area (m^2/g)	Mean pore diameter (nm)	Total pore volume (cm^3/g)
Spiolite (S.04)	326	45	0.8
Zeolite (Z.02)	472	52	1.2

3.3. Determining particle structure

As shown in Figure 3, the finer the particles, the less is the agglomeration of particles, and their crystallinity is clearer. Particle sizes distributed between 33.23 and 69.61 nm (Figure 3-d). The electronic microscope images show that the adsorption level, boundary between particles, accessibility to central atoms, and cation exchange increase due to the size reduction to Nano [32].

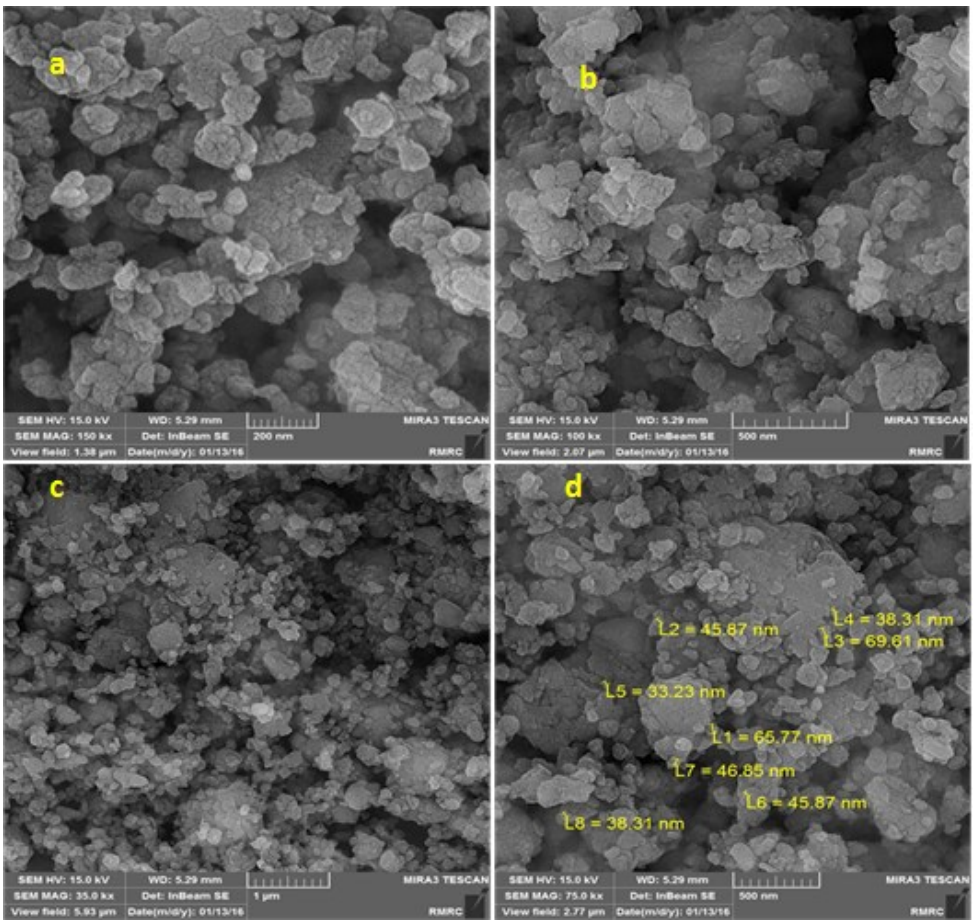

Figure 3. SEM images: Combination of sepiolite and zeolite nanoparticles after placing in a ball mill for 2 h (in the form of back scatter). Images a and b show a clear crystallinity of particles and prevention from their agglomeration due to size reduction of particles to Nano. b) shows particle size. Images c and d: Increasing adsorption; boundary between particles due to their nano-size.

3.4. IR spectroscopy

In order to confirm the presence of the toxic metals (Ni, Sb, and As) on the sorbents, FT-IR analyses were conducted before and after the adsorption process (Figure 4). The FT-IR spectra before and after the adsorption onto natural sepiolite and zeolite show a shift in the stretching vibration for the hydrogen bonds of OH at 3607 cm^{-1} (before adsorption) to 3589 cm^{-1} (after adsorption), for Si-O bonds at 1658 cm^{-1} (before adsorption) to 1647 cm^{-1} (after adsorption), for Si-O or Al-O at 1042 cm^{-1} (before adsorption) to 1035 cm^{-1} (after adsorption) [33-35]. This confirms that the OH, Si-O, and Al-O bonds are in connection with the adsorption of toxic metals.

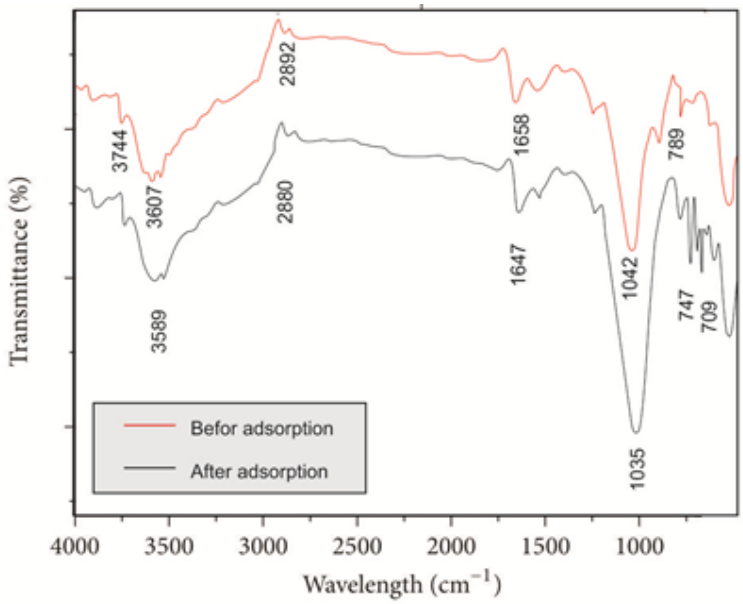

Figure 4. FT-IR spectra for natural sepiolite and zeolite before and after Ni, Sb, and As adsorption.

3.5. Studying effect of pH

A pH change can either increase or decrease the adsorption of the toxic elements by increasing or decreasing the H_3O^+ and OH^- ions in the solution. In the present work, some experiments were done to study the effect of pH on the performance of the adsorbents sepiolite and zeolite on nickel, arsenic, and antimony. As it can be seen in Figure 5, with an increase in pH between 2 and 6, the removal intensity of nickel (2.08-97.26%) and the adsorption capacity (0.002-0.11 mg/g) increase such that the highest amount of adsorption lies at pH 6. In an acidic pH, the surface of clay mineral is covered with $H3O^+$ ions, and Ni^{2+} ions can hardly compete with them to occupy the adsorption sites. An increase in pH reduces the competitive effect of the hydronium ions, and Ni^{2+} ions are adsorbed more easily in the empty places of the adsorbent, and thus the adsorption capacity increases [36]. The adsorbent used in this work has an experimental pH_{PZC} of 5.8. Therefore, at a pH value above pH_{PZC}, the net charge on the adsorbent becomes negative, while at a pH value below pH_{PZC}, the net surface charge becomes positive. Based on this, the negative charge increases with increase in the solution pH. Hence, the adsorbent gains a high charge resulting from the spread of isomorphous substitution in tetrahedral and octahedral sheets for sepiolite and zeolite. It can also be concluded that both the sepiolite and zeolite particles have a higher adsorption affinity to adsorb Ni^{2+} ions at high pH values. As the pH increases and the balance between the H_3O^+ and OH^- ions becomes equal, more positively charged Ni^{2+} ions in the solution are adsorbed on the negative clay surface, and thus the removal percentage of the Ni^{2+} ions increases. The toxic elements tend to form a precipitate at a pH value higher than 6.0, and therefore, the adsorption of Ni^{2+} ions by both the zeolite and sepiolite minerals are difficult to quantify at pH values higher than 6.0 [37].

Also pH reduction increases the positive charge on the clay mineral. Therefore, ions with negative charges such as arsenate are adsorbed. The highest adsorption intensity of this element (8.71%) and its adsorption capacity (0.01 mg/g) is found at pH 2. In Figure 5, the low adsorption of the arsenic ions can be attributed to the anionic competition in the mineral (such as phosphate and carbonate) [38]. The OH^- ions compete for the arsenate ions in the adsorption sites at high pH

values, and thus the adsorption capacity reduces due to the occupation of the adsorbent sites [39]. Nevertheless, the antimony ions are adsorbed at low pH values due to more hydrolysis in water and formation of the $Sb(OH)^{2+}$ complex with the oxygen atoms available in the clay mineral. Reduction in adsorption is seen at high pH values due to the competition of the hydroxylated groups of antimony, $Sb(OH)^-$, [40] such that an increase in the pH value reduces the adsorption intensity of antimony (38.36-98.33%) and the adsorption capacity (0.13-0.05 mg/g). Therefore, the favorable condition for the adsorption of this element is pH= 2 (Figure 5).

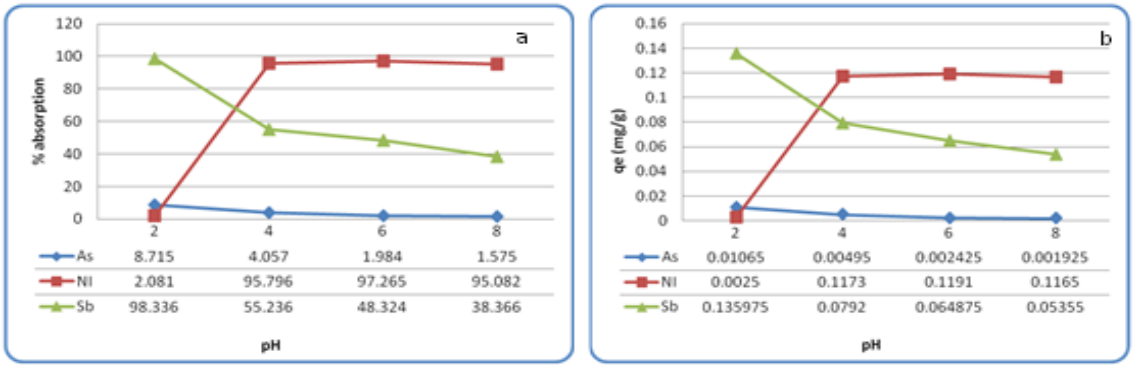

Figure 5. Graphs of pH effect on adsorption intensity and capacity of arsenic, nickel, and antimony. (a) adsorption intensity (b) adsorption capacity.

3.6. Studying effect of concentration

After determining the favorable pH value for adsorption of the toxic elements nickel, arsenic, and antimony, the effect of concentration on the adsorption of these elements was studied. As it can be seen in the graphs for the adsorption intensity and capacity (Figure 6), the increase in the concentration (1-50 mg/L) has reduced the adsorption intensity of nickel (99.44-51.10%), antimony (92.90-71.86%), and arsenic (32.85-17.76%); while the adsorption capacity has increased in nickel (0.01-0.6), antimony (0.02-0.26), and arsenic (0.08-2.17). Concerning the adsorption isotherm equations, at first, adsorption occurs on the surface of adsorbent, and the adsorption intensity increases but adsorption is taken inside the holes with increase in the concentration, reduction in the adsorption intensity, and increase in the adsorption capacity. The favorable concentration was obtained for adsorption of Ni^{2+}, C_e = 10 mg/L; Sb^{3+}, C_e = 10 mg/L; As^{5+}, C_e = 1 mg/L. In order to study the effect of the concentration of Ni^{2+} ions at pH 6, Sb^{3+} ions at pH 2, and As^{5+} ions at pH 2 on the amount of adsorption, the Eh-pH diagram can be studied for each element [41] (Figure 7). As it can be seen in Figure 7-a, formation of Ni^{2+} ions increase in the solution, and thus adsorption is increased. As shown in Figure 7-b, the stability of negative ions is reduced by reduction of pH (2), and $Sb(OH)_3$ solutions and $Sb(OH)^{2+}$ complexes created due to more hydrolysis of antimony and combination with oxygen atoms are increased, and thus the adsorption is more favorable. In Figure 7-c, the negative charge is reduced by PH reduction and increasing connection of the H^+ ions to arsenate (AsO_4^{3-}), and thus the stability of arsenate solutions such as $H_2AsO_4^-$ is increased, and thus adsorption is more favorable in the mineral surface.

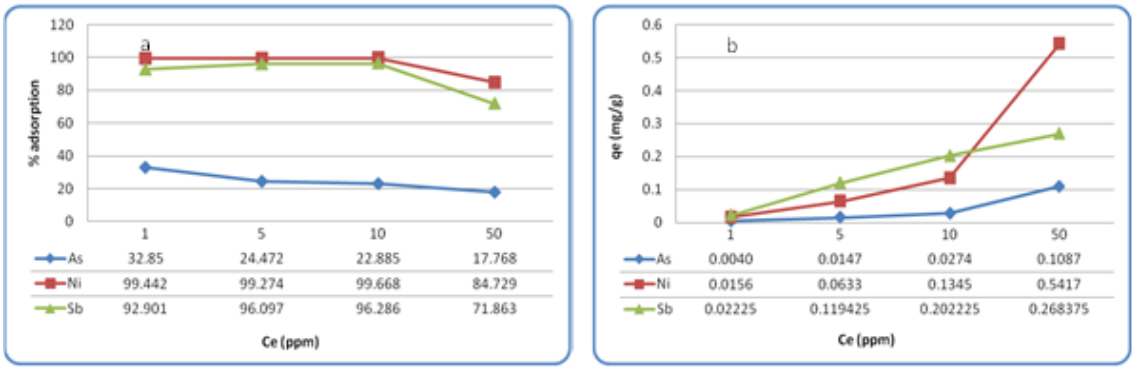

Figure 6. Graphs of effect of concentration on adsorption intensity and capacity of arsenic, nickel, and antimony. (a) Adsorption intensity (b) Adsorption capacity.

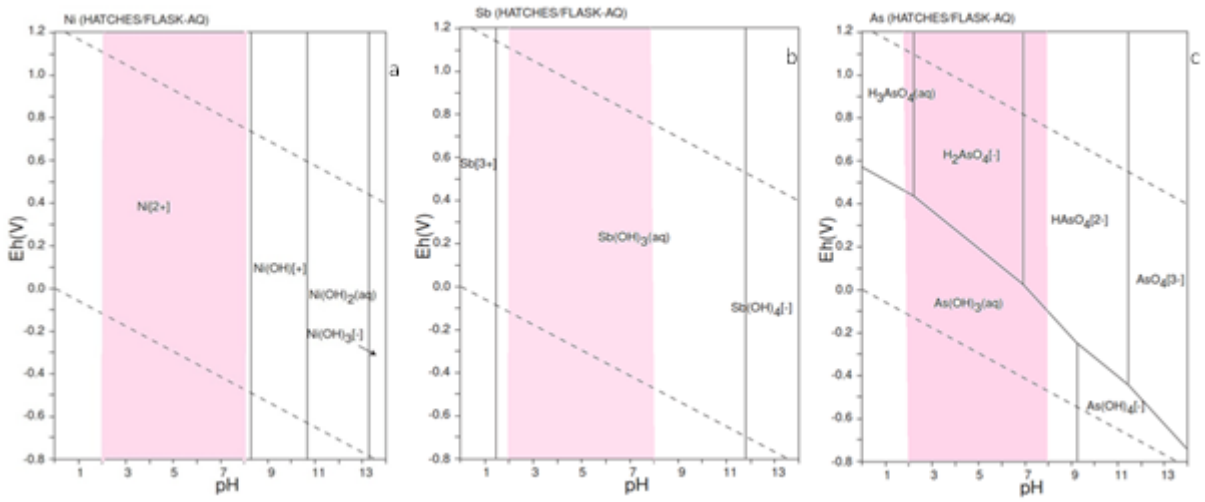

Figure 7. Eh-pH graph related to compounds (a) Ni^{2+} (b) Sb^{3+} and (C) As^{5+} at pH = 2-8 (Takeno, 2005).

3.7. Studying effect of adsorbent dose

An increasing adsorbent dose increases the proper site for adsorption but the adsorption capacity of the adsorbent is reduced by saturation of the adsorption surface [42]. As it can be seen in Figure 8, an increasing adsorbent dose (1-4 g/L) increases the adsorption intensity of nickel (70.26-99.25%) and an increasing adsorbent dose (1-2 g/L) increases the adsorption intensity of antimony (93.81-94.68%). It is while the adsorption intensity (93.01-92.02%) is reduced when the adsorbent dose lies between 3-4 g/L; the adsorption intensity of arsenic is increased (9.55-24.47%) as well. An increase in the adsorbent dose from 1 to 4 g/L, reduces the adsorption capacity of nickel (0.17-0.06), antimony (0.61-0.15), and arsenic (0.33-0.01) mg/g. The favorable condition for the removal of nickel, antimony, and arsenic is D = 4g/L, D = 2g/L, and D = 4g/L, respectively. The adsorption intensities of nickel and antimony are 99.25% and 94.68%, respectively, i.e. more than that in arsenic (24.47%), when the adsorbent dose increases. The reason is the accessibility of more exchange sites for these two elements compared to arsenic.

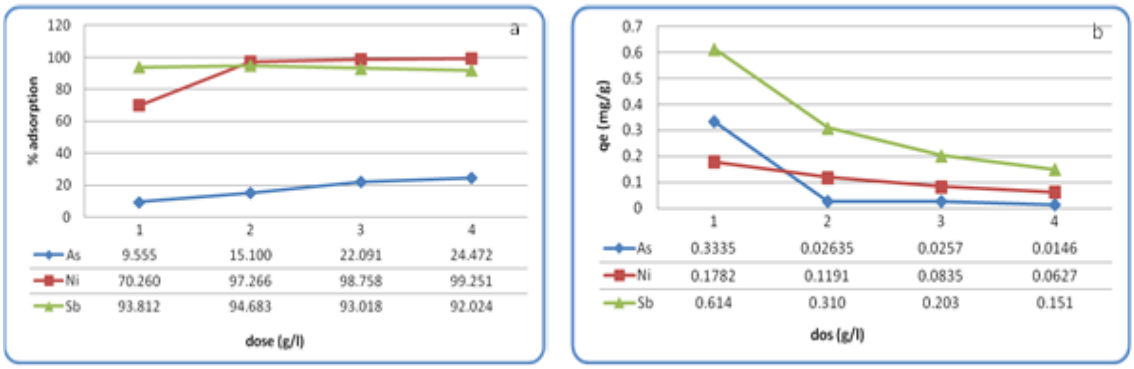

Figure 8. Graphs of effect of adsorbent dose on adsorption intensity and capacity of arsenic, nickel, and antimony. (a) Adsorption intensity (b) Adsorption capacity.

3.8. Studying effect of time

After identification of the pre-determined favorable parameters (pH, concentration, and adsorbent dose) for the three elements nickel, antimony, and arsenic, the graphs were plotted in order to study the effect of time (Figure 9). As it can be seen in this figure, the adsorption intensity of nickel (99.47-99.60%) is increased with increase in time (5-30 min) and it reduces within 45 minutes. The adsorption intensity of antimony (94.44-95.21%) is increased with increase in time (5-15 min) and it reduces between 30 and 45 min. The adsorption intensity of arsenic (25.39-49.60%) is increased between 5 and 15 minutes and it reduced between 30 and 45 minutes. The adsorption capacity of these elements is increased with increase in time and equilibrium. Then it is approximately stable after equilibrium and with increasing time. The ratio of concentration of ions remaining in the solution to

initial concentration of ions in the solution is stable and no adsorption occurs. In addition, with increase in time, the adsorption capacity of nickel, antimony, and arsenic is increased as 0.1270-0.1243 within 5-30 min, 0.278-0.280 within 5-15 min, and 0.0062-0.0032 within 5-15 min, respectively. As it can be seen in the graphs, the favorable times for the removal of nickel, antimony, and arsenic are T = 30 min, T = 15 min, and T = 15 min, respectively. The equilibrium is affected by some factors such as the properties of the adsorbent and adsorbate and the interaction between them [43]. Therefore, concerning the graph of adsorption capacity, it is clear that the cationic exchange of antimony (due to higher hydrolysis and charge) is faster than that for nickel within less time and its adsorption capacity is higher than that for nickel, while the adsorption capacity of As^{5+} is reduced due to the anion of arsenate. Substitution of Sb^{3+} is better than As^{5+} due to similarity to Al^{3+}, and the adsorption intensity is increased. Concerning the conducted experiments and investigation of the parameters in Table 1, the favorable condition and adsorption intensity of nickel, antimony, and arsenic are based upon Table 3.

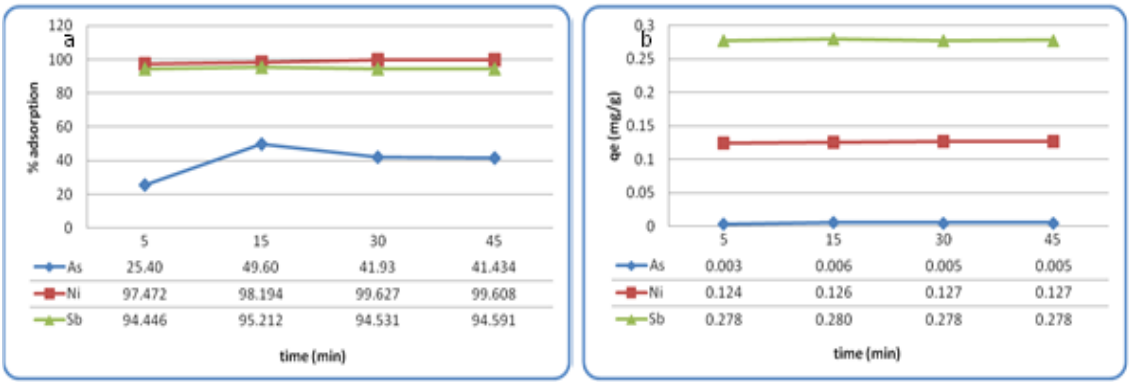

Figure 9. Graphs of effect of time on adsorption intensity and capacity of arsenic, nickel, and antimony. (a) Adsorption intensity (b) Adsorption capacity.

Table 3. Favorable parameters determined in the adsorption test.

Favorable paramete	Ni^{2+}	Sb^{3+}	As^{5+}
pH	6	2	2
Time (min)	30	15	15
Concentration (mg/L)	10	10	1
Adsorbent dose (g/L)	4	2	4
Adsorption intensity	99.61	95.39	35.87

4. Studying adsorption mechanism

The adsorption mechanism for clay minerals is based upon the adsorption and ion exchange. Clay minerals can adsorb toxic elements via ≡Si-O- and ≡Al-O- available at the edge of clay particles via ion exchange and formation of an inner-sphere complex [44]. The amount of adsorption of a substance on an adsorbent depends on many factors such as the quality of contact surface, temperature, and concentration and type of the adsorbate [45]. In addition, the amount of cations that substitutes clay minerals depends on the amount and concentration of the added salt, size and capacity of the exchanged cations, and amount of salt solvability. Generally, more concentration and less solvability cause the element cations to become more successful when competing with the cations available in the clay minerals. Basically, clay minerals prefer to adsorb cations with small size and more capacity. It is evident that all the above-mentioned factors are effective on the competition of cations rather than a unique factor [46]. Therefore, cation exchange and the Freundlich and Langmuir equations were used to study the adsorption mechanism.

4.1. Studying exchanged cations

4.1.1. Nickel cation exchange

The concentration of cations in the nickel nitrate solution was studied in the favorable conditions (concentration = 10 mg/L, adsorbent dose = 4g/L, time = 30 min). According to Figure 10, most cation exchanges of nickel are with sodium, and this is explainable due to the higher capacity of nickel. Then it is substituted with magnesium due to the smaller hydration radius and higher polarization of nickel than magnesium [46]. In Table 4, regarding the increasing concentration of

some elements in solution such as calcium (0.337-0.457 mg/L), potassium (0.054-0.082 mg/L), and aluminum (0.152-0.146 mg/L), the cationic exchange of nickel with these elements is low, resulting in the increasing adsorption of nickel by the adsorbent.

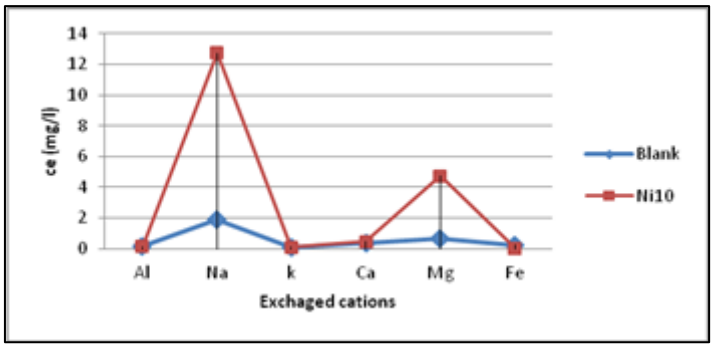

Figure 10. Comparing cations exchanged in nickel in blank solution and post-removal sample in favorable conditions (concentration = 10 mg/L, adsorbent dose = 4 g/L, time = 30 min, and pH = 6).

Table 4. Concentration of exchanged cations of nickel (mg/L) in blank solution and sample after removal.

Sample	Fe	Mg	Ca	k	Na	Al
Blank	0.24	0.634	0.337	0.054	1.923	0.146
Ni10	0.027	4.737	0.457	0.082	12.729	0.152

4.1.2. Cationic exchange of antimony

In order to study the cationic exchange of antimony, antimony chloride(III) was used with a concentration of 10 mg/L, an adsorbent dose of 2g/L, time = 15 min, and pH = 2. According to Figure 11, the highest cationic exchange of antimony was found with aluminum and magnesium. According to Table 5, the increasing concentration of aluminum (from 3.998 to 0.141 mg/L) and magnesium (from 0.018 to 72.28 mg/L) increases the exchange with magnesium. This may be due to the higher capacity of antimony than magnesium.

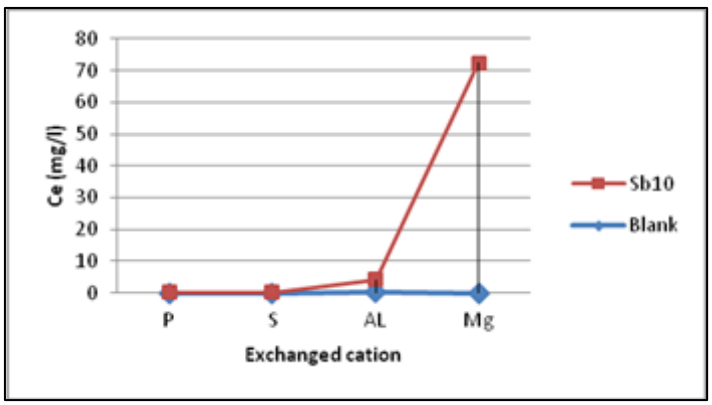

Figure 11. Comparing exchanged cations of antimony in blank solution and post-removal sample in favorable conditions (concentration = 10 mg/L, adsorbent dose = 2 g/L, time = 15 min, pH = 2).

Table 5. Concentration of exchanged cations of antimony (mg/L) in blank solution and post-removal sample.

Sample	Mg	Al	S	P
Blank	0.018	0.141	0.007	0.039
Sb10	72.282	3.998	0.064	0.074

4.1.3. Cationic exchange of arsenic

The cations exchanged in arsenate sodium hydrogen (v) were compared with the elements determined in the blank solution and arsenic in the favorable conditions (concentration = 1 mg/L, adsorbent dose = 4 g/L, time = 15 min, pH = 2). Based on Figure 12, the highest exchange of arsenic is found with the elements magnesium,

sodium, and calcium; this is explainable by the presence of magnesium in sepiolite and sodium in zeolite. The elements such as iron, silicium, and sulfur play fewer roles. According to Table 6, reduction of the phosphor concentration from 0.085 to 0.043 shows a higher adsorption than arsenic, substitution with aluminum, and a negative effect on the adsorption [39].

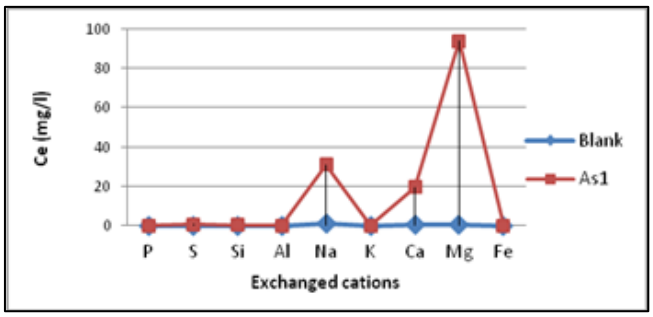

Figure 12. Comparing exchanged cations of arsenic in blank solution and post-removal sample in favorable conditions (concentration = 1 mg/L, adsorbent dose = 4 g/L, time = 15 min, pH = 2).

Table 6. Comparing concentration of exchanged cations (mg/L) of arsenic in blank solution and post-removal sample in favorable conditions.

Sample	Fe	Mg	Ca	K	Na	Al	Si	S	P
Blank	0.033	0.656	0.35	0.029	1.122	0.022	0.01	0.125	0.085
As1	0.048	93.843	19.697	0.172	31.02	0.013	0.518	0.649	0.043

4.2. Adsorption isotherm models

In order to study the adsorption mechanism, the Langmuir and Freundlich equations of the three elements nickel, antimony, and arsenic were used. The Freundlich graphs were obtained by plotting log qe against log C_e, and the Langmuir graphs were obtained by plotting 1/qe against $1/C_e$ (q_e is the adsorption capacity in mg/g and C_e is the equilibrium concentration of the solution) (Figure 13). When processing the curves, the points that are completely on the line show the most ideal state. If a solution with the same concentration is used, it will have the highest adsorption efficiency [47]. Coefficients of the Langmuir and Freundlich equations were calculated (Table 7). The correlation coefficient R^2 in the Langmuir (homogenous mono-layer adsorption) and Freundlich equations (heterogeneous multi-layer adsorption) for nickel, antimony, and arsenic follow these two equations ($0 < R^2 < 1$). Since the R^2 coefficient in the Langmuir equation for nickel (0.9895) and antimony (0.9689) is higher, the adsorption of these elements is mono-layer and homogeneous. The R^2 coefficient in the Freundlich equation for arsenic is higher (0.9995), and thus the adsorption is multi-layer and heterogeneous. Also comparing the adsorption capacities (q_m) of the three elements nickel (13.67 mg/g), antimony (5.26 mg/g), and arsenic (1.90 mg/g) shows more adsorption sites for nickel than for antimony and arsenic. By comparing coefficient b (adsorption power or energy in l/mg) among the Langmuir isotherms fornickel (-2.5), antimony (1.2), and arsenic (0.07), the adsorption powers of nickel and antimony are higher than arsenic. Concerning the amount of 0.0379 for nickel and 0.074 for antimony, the adsorption is irreversible and favorable, and it is favorable for arsenic (0.582). Regarding the Freundlich coefficients, the adsorption capacity (K_f in l/mg) in antimony, arsenic, and nickel is 8.19, 8.15, and 5.07, respectively, showing a higher adsorption of antimony in the Freundlich model due to a better substitution on the adsorbent. A proper cationic exchange with Al^{3+} was proved when studying the exchanged cations. The tendency for formation of complexes in arsenic can be one of the reasons for its good adsorption capacity. Studying the adsorption intensity (n) shows a reduction in the adsorption power in nickel (2.16), arsenic (1.22), and antimony (1.12). Nickel with a higher polarization and arsenic with a lower hydrolysis speed have higher adsorption powers than antimony. Of course, due to the amounts of n = 1-10, it can be said that adsorption is favorable in these three elements. The coefficient 1/n in the Freundlich equation shows the amount of heterogeneous adsorption. If $1/n < 1$, the bond energies increase with the surface density; if $1/n > 1$, the bond energies decrease with the surface density [48, 49]. Also if coefficient of heterogeneity is 1, the Freundlich equation will

change into a linear isotherm, showing the homogeneity of the adsorption sites. Values of 1/n for nickel, antimony, and arsenic are 0.46, 0.88, and 0.81, respectively, showing the homogeneous adsorption of all elements because 1/n > 0. Also this coefficient shows that the homogeneity of antimony and arsenic is higher than that for nickel.

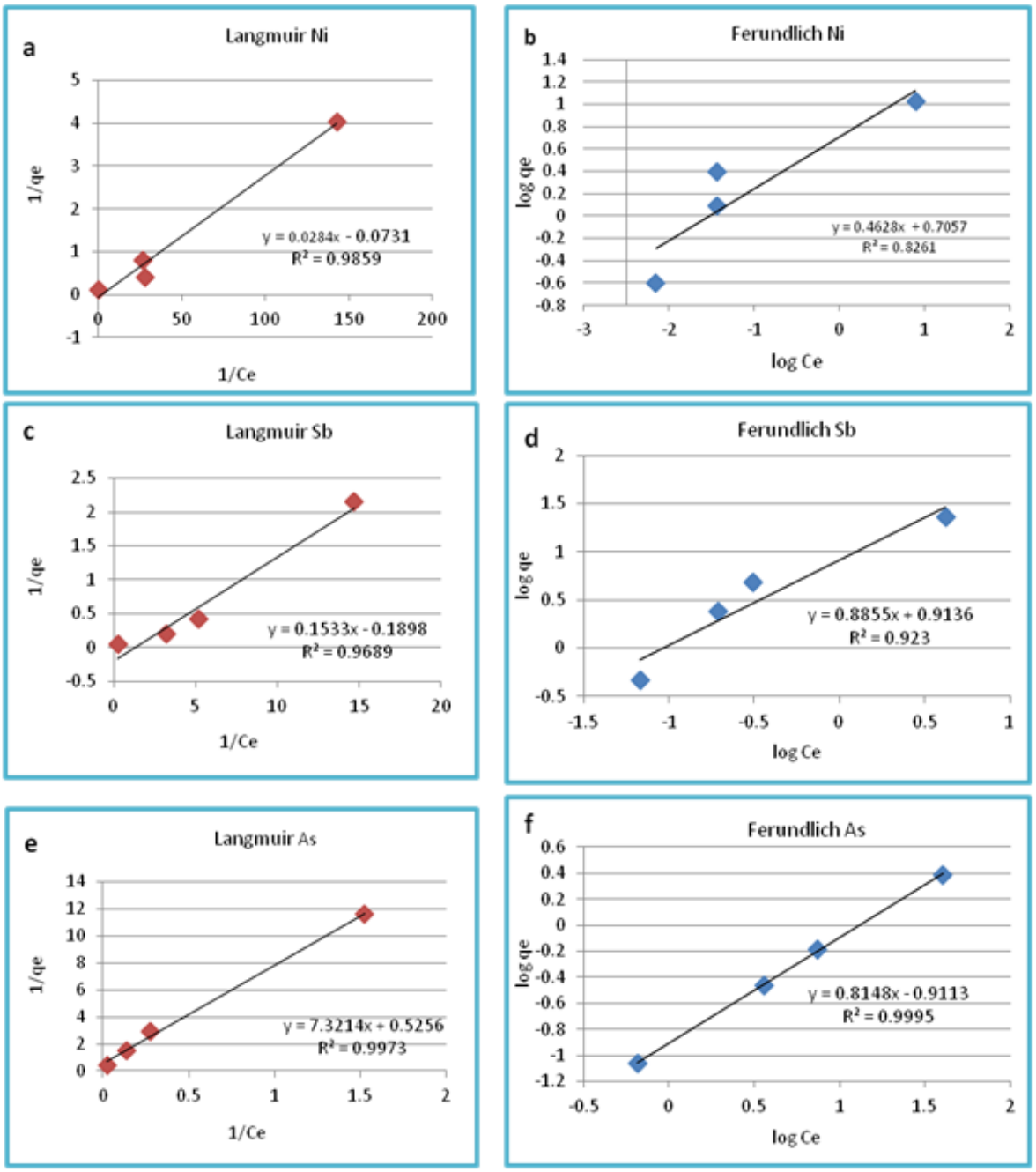

Figure 13. Adsorption isotherm equations. (a and b): Langmuir and Freundlich in nickel II adsorption, (c and d): Langmuir and Freundlich in adsorption of antimony III, (e and f): Langmuir and Freundlich in adsorption of arsenic V.

Table 7. Adsorption constants and correlation coefficients of Langmuir and Freundlich isotherms for the elements.

Isotherm equations	Langmuir				Freundlich			
Coefficients	$q_{m\ (mg/g)}$	$b_{\ (L/mg)}$	R_L	R^2	$K_{f\ (mg/g)}$	$n_{\ (L/mg)}$	1/n	R^2
Ni^{2+}	-13.6798	-2.5739	0.037	0.9859	5.0780	2.1607	0.4628	0.8261
Sb^{3+}	-5.2687	-1.2380	0.074	0.9689	8.1959	1.1293	0.8855	0.9230
As^{5+}	1.9025	0.0717	0.582	0.9973	-8.1526	1.2272	0.8148	0.9995

4.3. Adsorption kinetics

The adsorption behavior of an adsorbent on an adsorbate can be studied using the adsorption kinetics. The adsorption efficiency is the change in adsorption per unit time, and it is the key parameter used to describe the absorption efficiency [50]. The kinetic parameters give important information for optimizing, designing, and modeling the adsorption process. Several kinetic models are available in order to investigate the adsorption mechanisms. The pseudo-first-order model was the first model used for the sorption of a liquid/solid system based on the solid capacity [51, 52]. In most cases, the pseudo-first-order equation is the best match for the whole range of contact time. k_1 values were calculated from the plot of $\log(q_e\text{-}q)$ versus t for different element ion adsorption studies. The pseudo-second-order reaction model is based on the adsorption capacity depending on time [53]. The equation constants are determined by plotting t/q_t against t. The mechanism involved in the adsorption process is identified using the intra-particle diffusion model. According to this model, proposed by Weber and Morris, the initial rate of intra-particle diffusion is calculated by plotting q against $t^{1/2}$ [54]. As it can be seen in Figure 14, by plotting q_t versus t, the theoretical q_e, k_1, k_2, and R^2 values can be calculated. As it can be seen in Table 8, the high R^2 values in the range of 0.94-0.99 and the good conformity of the theoretical values with the experimental values expose that the kinetic mechanism of adsorption of nickel, antimony, and arsenic on natural sepiolite and zeolite sorbents can be explained satisfactorily by the pseudo-second-order model.

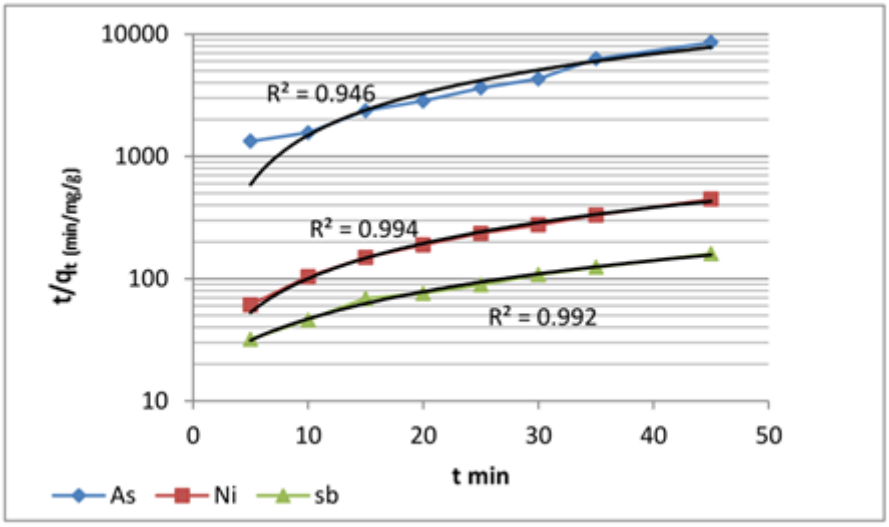

Figure 14. Pseudo-second-order kinetic plots obtained for Ni, As, and Sb sorption by natural sepiolite and zeolite nanoparticles sorbent.

Table 8. Kinetic constants and correlation coefficients of all kinetic models.

	Pseudo-first-order			Pseudo-second-order		
	K_1 (min^{-1})	q_e (mg/g)	R^2	K_2 (g/mg min)	q_e (mg/g)	R^2
Ni^{2+}	0.067	79.25	0.951	0.011	332.1	0.994
As^{5+}	0.059	80.65	0.814	0.006	234.5	0.946
Sb^{3+}	0.105	39.33	0.907	0.318	174.3	0.992

4.4. Adsorption thermodynamics

The changes in enthalpy (ΔH) and entropy (ΔS) were calculated based on the distribution coefficients
($K_D = q_e/c_e$) obtained at 20, 25, 30, 35, 40, 45, and 50 °C and using the van't Hoff's equation [55] as follow:

$$\ln K_D = \frac{\Delta S}{R} - \frac{\Delta H}{RT} \quad (7)$$

where K_D is the distribution coefficient (mL/g), ΔH° is the enthalpy change, ΔS° is the entropy change, T is the temperature (K), and R is the universal gas constant (8.314 J/mol.K). The free energy change (ΔG°) is determined usingthe following equation:

$$\Delta G^\circ = \Delta H^\circ - T\,\Delta S^\circ \quad (8)$$

Based on Eq. (8), the ΔH° and ΔS° parameters can be calculated from the slope and intercept of the

plot of lnKD *vs.* 1/T, respectively (Figure 15). The values for ΔG°, ΔH°, and ΔS° are given in Table 9 for the Ni, As, and Sb absorption on natural sepiolite and zeolite. The negative values for ΔG° indicate that the adsorption process for the three toxic elements (Ni, As, and Sb) is feasible and spontaneous. It was observed that the values became more negative with increase in the temperature. The positive values for ΔH° confirm the endothermic nature of the adsorption of the nickel, antimony, and arsenic ions on natural sepiolite and zeolite in the temperature range of 20-50 °C. The positive ΔS° values indicate the affinity of the adsorbent for the nickel and arsenic ions. Moreover, the calculated negative ΔS° value for antimony (–94.2 J mol^{-1} K^{-1}) indicate a decrease in randomness during the adsorption.

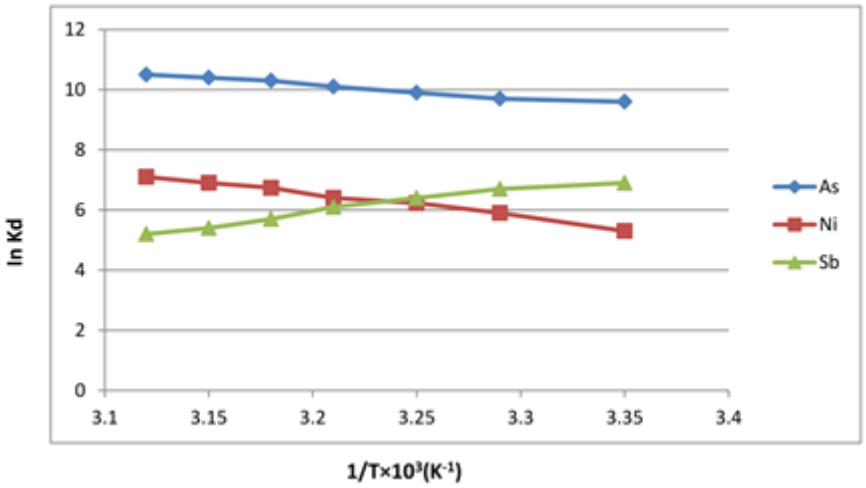

Figure 15. Plots of lnK_D *vs.* 1/T for nickel antimony and arsenic adsorption on natural sepiolite and zeolite nanoparticles.

Table 9. Thermodynamic parameters for adsorption of nickel, antimony, and arsenic ions on natural sepiolite and zeolite.

Ions	ΔG° (kJ/mol)							ΔH° (kJ/mol)	ΔS° (J/mol.K)
	20°C	25°C	30°C	35°C	40°C	45°C	50°C		
Ni^{2+}	-44.31	-44.85	-45.67	-45.92	-46.11	-47.65	-48.04	27.15	146.11
As^{5+}	-35.12	-36.07	-36.44	-37.27	-38.44	-38.84	-39.17	11.88	158.04
Sb^{3+}	-13.32	-13.80	14.75	15.48	16.0	16.35	16.9	48.1	-94.2

5. Conclusions

The low-cost clay minerals sepiolite and zeolite were used in this study to remove nickel(II), antimony(III), and arsenic(V) from synthetic wastewater. The adsorption kinetic and equilibrium of these toxic ions were determined using various operating parameters such as the solution pH. dosage of adsorbent, contact time, temperature, and initial element concentrations using the low-cost natural minerals in a batch operation mode. The optimal conditions for adsorption of nickel by natural sepiolite and zeolite were pH = 6, initial Ni concentration = 10 mg/L, adsorbent dose = 4 g/L, and removal time = 30 min. Also the optimum conditions for the adsorption of antimony and arsenic were obtained to be (10 and 1 mg/L) of the initial ion concentration, (2 and 4 g/L) of the adsorbent dose, pH = 2, and time = 15 min for both ions, respectively. Adsorption of nickel and antimony via the sepiolite and zeolite nanoparticles is more favorable in the Langmuir isotherm, while arsenic shows a better adsorption in the Freundlich isotherm. After kinetic evaluation, it became obvious that the pseudo-second-order kinetic reaction model represented the data better for both toxic ion removal processes. The values obtained for the thermodynamic parameters involved show that adsorption of nickel, antimony, and arsenic was endothermic and spontaneous in nature. High adsorption capacity, ease of preparation, low-cost, and high adsorption/desorption stability make natural sepiolite and zeolite promising sorbents for the elimination of nickel(II), antimony(III), and arsenic(V) ions from synthetic wastewaters.

Acknowledgments
We are grateful to the reviewers of this paper for their constructive reviews, which significantly improved the quality of this paper. The authors also appreciate the support received from the Islamic Azad University, Mashhad Branch.

References

[1]. Mateo-Sagasta, J., Zadeh, S.M., Turral, H. and Burke, J. (2017).Water pollution from agriculture: a global review. Executive summary. Rome, Italy: FAO Colombo, Sri Lanka: International Water Management Institute (IWMI). CGIAR Research Program on Water, Land and Ecosystems (WLE).

[2]. Charkhabi, A.H., Sakizadeh, M. and Rafiee, G. (2005). Seasonal Fluctuation in Heavy Metal Pollution in Iran´ s Siahroud River-A Preliminary Study (7 pp). Environmental Science and Pollution Research. 12: 264-270.

[3]. Singh, V.P., Yadav, S. and Yadava, R.N. (2018). Hydrologic Modeling: Select Proceedings of ICWEES-2016. Springer.

[4]. Hamed Mosavian, M.T., Khazaei, I. and Aliabadi, M. (2012). Use of Sawdust of Aspen Tree for the Removal of Chromium (VI) from Aqueous Solution. Iranian Journal of Earth Sciences. 4: 25-30.

[5]. Jaishankar, M., Tseten, T., Anbalagan, N., Mathew, B.B. and Beeregowda, K.N. (2014). Toxicity, mechanism and health effects of some heavy metals. Interdisciplinary toxicology. 7: 60-72.

[6]. Lu, F. and Astruc, D. (2018). Nanomaterials for removal of toxic elements from water. Coordination Chemistry Reviews. 356: 147-164.

[7]. Boente, C., Sierra, C., Rodríguez-Valdés, E., Menéndez-Aguado, J. and Gallego, J. (2017). Soil washing optimization by means of attributive analysis: Case study for the removal of potentially toxic elements from soil contaminated with pyrite ash. Journal of cleaner production. 142: 2693-2699.

[8]. Gunatilake, S. (2015). Methods of removing heavy metals from industrial wastewater. Methods. 1.

[9]. Usman, K., Al-Ghouti, M.A. and Abu-Dieyeh, M.H. (2018). Phytoremediation: Halophytes as Promising Heavy Metal Hyperaccumulators.

[10]. Otero, M., Rozada, F., Morán, A., Calvo, L. and García, A. (2009). Removal of heavy metals from aqueous solution by sewage sludge based sorbents: competitive effects. Desalination. 239: 46-57.

[11]. Zhang, X. and Wang, X. (2015). Adsorption and desorption of nickel (II) ions from aqueous solution by a lignocellulose/montmorillonite nanocomposite. PLOS One. 10: e0117077.

[12]. Pathania, D., Sharma, S. and Singh, P. (2017). Removal of methylene blue by adsorption onto activated carbon developed from Ficus carica bast. Arabian Journal of Chemistry. 10: S1445-S1451.

[13]. Bailey, S.E., Olin, T.J., Bricka, R.M. and Adrian, D.D. (1999). A review of potentially low-cost sorbents for heavy metals. Water research. 33: 2469-2479.

[14]. Adare, A., Afanasiev, S., Aidala, C., Ajitanand, N., Akiba, Y., Akimoto, R., Al-Ta'ani, H., Alexander, J., Angerami, A. and Aoki, K. (2012). Evolution of π 0 Suppression in Au+ Au Collisions from s NN= 39 to 200 GeV. Physical review letters. 109: 152301.

[15]. Galan, E. (1996). Properties and applications of palygorskite-sepiolite clays. Clay Minerals. 31: 443-453.

[16]. Ismadji, S., Soetaredjo, F.E. and Ayucitra, A. (2015). Natural clay minerals as environmental cleaning agents**.** In Clay materials for environmental remediation. Springer. pp. 5-37.

[17]. Breck, D.W. (1984). Zeolite molecular sieves: structure, chemistry and use. Krieger.

[18]. Moliner, M., Martínez, C. and Corma, A. (2015). Multipore zeolites: synthesis and catalytic applications. Angewandte Chemie International Edition. 54: 3560-3579.

[19]. Erdem, E., Karapinar, N. and Donat, R. (2004). The removal of heavy metal cations by natural zeolites. Journal of colloid and interface science. 280: 309-314.

[20]. Reeve, P.J. and Fallowfield, H.J. (2018). Natural and surfactant modified zeolites: A review of their applications for water remediation with a focus on surfactant desorption and toxicity towards microorganisms. Journal of environmental management. 205: 253-261.

[21]. Savage, N. and Diallo, M.S. (2005). Nanomaterials and water purification: opportunities and challenges. Journal of Nanoparticle research. 7: 331-342.

[22]. Hamed Mosavian, M.T., Khazaei, I. and Aliabadi, M. (2009). Removal of chromium (VI) from aqueous solution by adsorption using cousinia eryngioides boiss and activated carbon. Iranian Journal of Earth Sciences. 1: 35-43.

[23]. Mckay, G. (1995).Use of Adsorbents for the Removal of Pollutants from Wastewater. CRC press.

[24]. Lopez-Ramon, M.V., Stoeckli, F., Moreno-Castilla, C. and Carrasco-Marin, F. (1999). On the characterization of acidic and basic surface sites on carbons by various techniques. Carbon. 37: 1215-1221.

[25]. Garcıa-Sánchez, A., Alastuey, A. and Querol, X. (1999). Heavy metal adsorption by different minerals: application to the remediation of polluted soils. Science of the total environment. 242: 179-188.

[26]. Darder, M., Colilla, M. and Ruiz-Hitzky, E. (2003). Biopolymer− clay nanocomposites based on

chitosan intercalated in montmorillonite. Chemistry of Materials. 15: 3774-3780.

[27]. Shahmohammadi-Kalalagh, S. (2011). Isotherm and kinetic studies on adsorption of Pb, Zn and Cu by kaolinite. Caspian Journal of Environmental Sciences. 9: 243-255.

[28]. Langmuir, I. (1918). The adsorption of gases on plane surfaces of glass, mica and platinum. Journal of the American Chemical society. 40: 1361-1403.

[29]. Shah, B., Shah, A. and Shah, P. (2011). Sorption isotherms and column separation of Cu (II) and Zn (II) using ortho substituted benzoic acid chelating resins. Archives of Applied Science Research. 3: 327-341.

[30]. Freundlich, H. (1922).Kapillarchemie. Akademische Verlagsgesellschaft.

[31]. Dada, A., Olalekan, A., Olatunya, A. and Dada, O. (2012). Langmuir, Freundlich, Temkin and Dubinin–Radushkevich isotherms studies of equilibrium sorption of Zn2+ unto phosphoric acid modified rice husk. IOSR Journal of Applied Chemistry. 3: 38-45.

[32]. Sen, T. (2017). Clay Minerals: Properties, Occurrence and Uses.

[33]. Orha, C., Pop, A., Lazau, C., Grozescu, I., Tiponut, V. and Manea, F. (2012). Silver doped natural and synthetic zeolites for removal of humic acid from water. Environmental Engineering & Management Journal (EEMJ). 11 (3).

[34]. Medina, A., Gamero, P., Querol, X., Moreno, N., De León, B., Almanza, M., Vargas, G., Izquierdo, M. and Font, O. (2010). Fly ash from a Mexican mineral coal I: Mineralogical and chemical characterization. Journal of hazardous materials. 181: 82-90.

[35]. Junaid, A., Rahman, M., Rocha, G., Wang, W., Kuznicki, T., McCaffrey, W. and Kuznicki, S. (2014). On the role of water in natural-zeolite-catalyzed cracking of athabasca oilsands bitumen. Energy & Fuels. 28: 3367-3376.

[36]. Li, L.Y. and Li, R.S. (2000). The role of clay minerals and the effect of H+ ions on removal of heavy metal (Pb2+) from contaminated soils. Canadian geotechnical journal. 37: 296-307.

[37]. Mckay, G., Bino, M. and Altamemi, A. (1985). The adsorption of various pollutants from aqueous solutions on to activated carbon. Water Research. 19: 491-495.

[38]. Chiban, M., Lehutu, G., Sinan, F. and Carja, G. (2009). Arsenate removal by Withania frutescens plant from the south–western Morocco. Environ Eng Manage J. 8: 1377-1383.

[39]. De Esparza, M. (2006). Removal of arsenic from drinking water and soil bioremediation. In Natural arsenic in groundwater of Latin America international congress. pp. 20-24.

[40]. Targan, Ş., Tirtom, V.N. and Akkuş, B. (2013). Removal of antimony (III) from aqueous solution by using grey and red Erzurum clay and application to the Gediz River sample. ISRN Analytical Chemistry.

[41]. Takeno, N. (2005). Atlas of Eh-pH diagrams. Geological survey of Japan open file report. 419: 102.

[42]. Ghosh, D. and Bhattacharyya, K.G. (2002). Adsorption of methylene blue on kaolinite. Applied clay science. 20: 295-300.

[43]. Gupta, S.S. and Bhattacharyya, K.G. (2011). Kinetics of adsorption of metal ions on inorganic materials: a review. Advances in colloid and interface science. 162: 39-58.

[44]. Celis, R., Hermosin, M.C. and Cornejo, J. (2000). Heavy metal adsorption by functionalized clays. Environmental science & technology. 34: 4593-4599.

[45]. Tchobanoglous, G., Burton, F.L. and Stensel, H. (1991). Wastewater engineering. Management. 7: 1-4.

[46]. Vepraskas, M.J., Faulkner, S. and Richardson, J. (2001). Redox chemistry of hydric soils. Wetland soils: Genesis, hydrology, landscapes, and classification. pp. 85-106.

[47]. Venkatesha, T., Viswanatha, R., Nayaka, Y.A. and Chethana, B. (2012). Kinetics and thermodynamics of reactive and vat dyes adsorption on MgO nanoparticles. Chemical engineering journal. 198: 1-10.

[48]. Toth, J. (2002). Adsorption. CRC Press.

[49]. Azizian, S. (2004). Kinetic models of sorption: a theoretical analysis. Journal of colloid and Interface Science. 276: 47-52.

[50]. Chen, Y., Lan, T., Duan, L., Wang, F., Zhao, B., Zhang, S. and Wei, W. (2015). Adsorptive removal and adsorption kinetics of fluoroquinolone by nano-hydroxyapatite. PlOS one. 10: e0145025.

[51]. Lagergren, S. (1898). Zur theorie der sogenannten adsorption geloster stoffe. Kungliga svenska vetenskapsakademiens Handlingar. 24: 1-39.

[52]. Yuh-Shan, H. (2004). Citation review of Lagergren kinetic rate equation on adsorption reactions. Scientometrics. 59: 171-177.

[53]. Ho, Y.S. and McKay, G. (1999). Pseudo-second order model for sorption processes. Process biochemistry. 34: 451-465.

[54]. Weber, W.J. and Morris, J.C. (1963). Kinetics of adsorption on carbon from solution. Journal of the Sanitary Engineering Division. 89: 31-60.

[55]. Elwakeel, K.Z., El-Sayed, G.O. and Darweesh, R.S. (2013). Fast and selective removal of silver (I) from aqueous media by modified chitosan resins. International Journal of Mineral Processing. 120: 26-34.

ارزیابی عملکرد نانو ذرات طبیعی سپیولیت و زئولیت برای حذف نیکل، آنتیموان و آرسنیک از فاضلاب مصنوعی

رحیم دبیری* و الهه امیری شیراز

گروه زمین‌شناسی، واحد مشهد، دانشگاه آزاد اسلامی، مشهد، ایران

ارسال ۲۰۱۸/۶/۲۴، پذیرش ۲۰۱۸/۸/۲۵

* نویسنده مسئول مکاتبات: r.dabiri@mshdiau.ac.ir

چکیده:

در این پژوهش به مطالعه جذب عناصر سمناک از فاضلاب مصنوعی به روش جذب دسته‌ای پرداخته می‌شود. کانی‌های رسی با توجه به سطح ویژه و پتانسیل جذب بالا، به عنوان جاذب‌های ارزان قیمت محسوب می‌شوند. در این پژوهش به منظور حذف نیکل (II)، آنتیموان (III) و آرسنیک (V) از کانی‌های طبیعی ارزان قیمت سپیولیت (از معدن الیتو واقع در شمال شرق ایران) و زئولیت (از معدن افتر واقع در شمال ایران) بهره گرفته شده است. آزمایش‌های جذب توسط تغییر در میزان غلظت اولیه عناصر، pH، زمان جذب و دوز جاذب انجام شده است. داده‌های ایزوترم تجربی با استفاده از معادلات لانگمویر و فروندلیچ مورد تجزیه و تحلیل قرار گرفته است. با توجه به ضریب R^2 بالاتر لانگمویر در عناصر نیکل و آنتیموان، مکانیسم جذب این عناصر تک لایه و همگن می‌باشند. همچنین بر اساس مدل جذب فروندلیچ، جذب آرسنیک چند لایه و ناهمگن است. بررسی سینتیک واکنش نیز نشان می‌دهد، فرآیند جذب نیکل، آنتیموان و آرسنیک از مدل سینتیک شبه درجه دوم تبعیت می‌کند. پارامترهای ترمودینامیکی بیانگر آن است که فرایندهای جذب گرمازا بوده و با کاهش دما خودبه‌خودی است. بر اساس نتایج تجربی، می‌توان نتیجه گرفت که سپیولیت و زئولیت طبیعی دارای قابلیت کاربردی به عنوان یک جاذب کارآمد برای حذف عناصر سمناک از فاضلاب مصنوعی است.

کلمات کلیدی: جذب، نانو ذرات سپیولیت و زئولیت، عناصر سمناک، ایزوترم، سینتیک.